全球地震波伝播シミュレーション

課題責任者

坪井誠司 海洋研究開発機構 付加価値情報創生部門 地球情報基盤センター

著者

坪井誠司*[1], Rhett Butler*[2]

*[1]海洋研究開発機構　付加価値情報創生部門　地球情報基盤センター, *[2] University of Hawai'i

地震震源の対蹠点で核ーマントル境界を回折して伝播する地震波の Pdiff 波を観測することで、核ーマントル境界の構造を推定することができる。さらに、マントル内で同じ波線を共有する PKP_{AB} 波との走時差を用いることでマントルの不均質構造の影響を取り除くことができる。PKP_{AB} 波と Pdiff 波の走時差を調べるときに Pdiff 波が対蹠点近傍で極での位相ずれを起こしているかを検証することが重要である。ここでは核ーマントル境界を通過する地震波の観測波形についてスペクトル要素法を用いた理論地震波形記録を計算し、対蹠点における Pdiff 波のモデル化を行った。

キーワード：数値波形計算、地震波動、地球外核ーマントル境界

1. はじめに

地震の対蹠点では、地球はほぼ球形のレンズのように振る舞い、地震とその対蹠点の間の直径を中心に軸対称の領域を通して地震エネルギーを集中させる。対蹠点における観測[1-8]は、実体波と自由振動の観測を補完して他の場所では観測できない地球の内部構造を明らかにする可能性がある。

PKIKP 波は地球の中心を直進するが、地震から正反対の対蹠点への最速経路ではない。むしろ、核ーマントル境界（CMB）の周りで回折された P 波（Pdiff）がより早く到着する。核による P 波の回折は Gutenberg によって指摘された[9]。数年後、Gutenberg[10]は、「反中心付近のエネルギーの集中の影響として…したがって、大地震では、回折波は反中心まで十分に観測できる」と仮定した。

2. データ

対蹠点における Pdiff の最初の観測は、1968 年にスペインの PTO で震央距離 179.25° で観測された MS =7.1 ニュージーランドの地震について、Rial[1]によって行われ、Rial&Cormier[2]によってモデル化された。Butler[3]は、PKIKP-Pdiff の走時時間差と Mw = 7.9 のミナハサ地震の対蹠点である PTGA（179.9°）での分極を測定した。本研究は Butler[4]を拡張し、アルジェリアの TAM 観測点と中国の QIZ 観測点の対蹠点となる 2 つの大地震に対して、Pdiff の基準として PKP_{AB} を使用して差分走時を測定した。これら 3 つの地震の Pdiff のフレネルゾーンは、核ーマントル境界領域の 99%以上をカバーしている。

3. Pdiff と核-マントル境界領域

歴史的な理由から D″と呼ばれる最下部のマントルは、地球の液体の外核に接している。この領域は著しく横方向に不均一であることがわかっており、実体波によってサンプリングされたさまざまな領域の負、ほぼゼロ、または正の地震速度勾配を特徴としている。これまでの Pdiff の観測は、震央距離が 160 度以下の場合に限られていた。

４．差分走時と位相変化

差分走時の利点は、共通のマントルの不均質性が解消されるという点にある。この研究では、PKP_{AB} を基準として用いており、マントル内の同じ波線を Pdiff と共有している。 PKP_{AB} が核で屈折する場合、Pdiff は核の周りで回折し、 CMB からマントルを通過する際に、両方の波が再び合流する。

PKIKP は対蹠点で増幅されず、伝播で位相変化も発生しない。 PKP_{AB} と Pdiff は共に増幅される[2-3]。PKP_{AB} の、伝播時の位相変化はπ/ 2 ラジアンであり、180° でπ/ 4 ラジアンの極位相シフト[11-13]が追加される。対蹠点でのπ/ 4 極位相変化は、対蹠点に近づく（Δ<180°）波動場（0° シフト）と対蹠点から離れる（Δ> 180°）波動場（90° シフト）の合算である。対蹠点（Δ = 180°）では、正味のπ/ 4 または 45° の位相変化となる。

差分走時の決定は、比較する地震波の到着で位相が一致することが必要となる。波形を比較するには、位相を共通の基準に調整する必要があり、したがって、重要な問題は、Pdiff が PKP_{AB} と同じπ/ 4 ラジアンの極位相変化を被るかどうかという点である。

5. Pdiff極位相変化の計算

Brune[11]とGilbert[14]は、正規モード解における極位相変化の適用性について議論を行った。Pdiffは正規モード解の重ね合わせと見なすことができるので、極位相変化は当然発生する。Hill[12]は、極位相の変化（軸苛性）を波線理論による高周波現象と考えた。Pdiffの極位相変化についての理論的研究はないので、スペクトル要素法[5、15-17]を使用して数値的に問題に取り組むこととした。

PREMモデルに対して計算されたPdiffとPKP_{AB}を直接比較して、等方性爆発震源と震央距離180° の対蹠点で、漸近的な周波数依存の位相を暗黙に含めた。

Pdiff波の理論地震記録は、合計135億個の格子点を持つメッシュを使用した。これは、地球の表面で2.0kmの格子点間隔に対応し、3.5秒の精度で理論地震波形記録を提供する。

6. Pdiff極位相変化の測定

この計算の結果は、図1aに示した。Pdiffは、極性位相がπ／ 4シフトしている（45° ）か、シフトしていない（0° ）かのいずれかである。最初に、[PKP_{AB}] _（−π／ 2）は−π／ 2ラジアンだけ位相シフトし（PKP_{AB}伝播コースティックスを考慮するため）、Pdiffと直接比較した。極位相シフトの補正は行われていない。[PKP_{AB}] _（−π／ 2）は暗黙的にπ／ 4極位相シフトを含むため、この波形がPdiff波形と一致することは、Pdiffが暗黙的に同じ極位相シフトを含むことが必要である。一方、[PKP_{AB}] _（−3π／ 4）は、極位相シフトと伝播コースティックスの両方を補正するため、位相シフトは−3π／ 4ラジアンである。 [PKP_{AB}] _（−3π／ 4）はPKP_{AB}（π／ 4）の極位相シフトを明示的に反転するため、Pdiffと[PKP_{AB}] _（−3π／ 4）との一致が良いことは、Pdiffに極位相シフトがないことを意味している。しかしながら、一致は良くないため、Pdiffには極性の位相シフトがあると推測される。

瞬間位相[18]を図1bにプロットした。図1aの比較と同様に、[PKP_{AB}] _（−π／ 2）はPdiffと重なっており、同じ位相関係を共有している。さらに、[PKP_{AB}] _（−3π／ 4）の一致はよくない。したがって、瞬間位相は、[PKPAB] _（−π／ 2）がPdiffと重なっており、両方が同じ極位相シフトを共有することを示している。

これらの結果からPdiffがPKP_{AB}と同じπ／ 4ラジアンの極位相変化を被ることが結論できる。

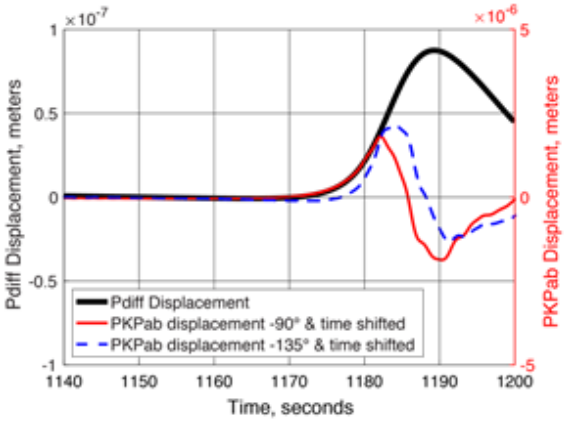

図 1a 対蹠点（Δ = 180° ）での P_diff の潜在的な極位相シフトを解決するために、スペクトル要素法（SEM）によって球対称 PREM 地球モデルに対して計算した理論波形を比較した。定性的には、[PKP_{AB}] _（−π／ 2）は最初に P_diff と重なっているが、[PKP_{AB}] _（−3π／ 4）とは重ならない。 P_diff と[PKP_{AB}] _（−π／ 2）の波形の一致は、D“に起因する可能性が高い PKP_{AB} の短周期成分が到着すると、約 15 秒後に悪くなる。

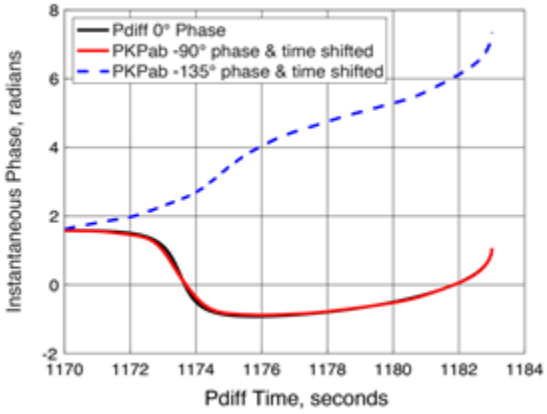

図 1b 変位成分から導出された瞬間位相を示した。P_diff（黒）と[PKP_{AB}] _（−π／ 2）（赤）は互いに重なっている。しかしながら、P_diff と[PKP_{AB}] _（−3π／ 4）（青い点線）はよく一致しない。したがって、P_diff と[PKP_{AB}] _（−π／ 2）は、P_diff の開始時にほぼ同じ瞬間位相を持ち、対蹠点での（π／ 4）の P_diff 極性位相シフトを裏付けている。

文献

[1] Rial, J. A., 1979. Seismic waves at the epicenter's antipode, Doctoral Dissertation Caltech, Pasadena.

[2] Rial, J. A., and V. F. Cormier, 1980. Seismic waves at the epicenter's antipode, *J. Geophys. Res.*, *85*, 2661–2668.

[3] Butler, R., 1986. Amplitudes at the antipode, *Bulletin of the Seismological Society of America, 76*, 1355–1365.

[4] Butler, R., 1998. Antipodal observations of the inner-outer core boundary and diffracted P, *EOS Trans. AGU suppl*., 79.

[5] Butler, R., and S. Tsuboi, 2010. Antipodal seismic observations of temporal and global variation at Earth's inner-outer core boundary, *Geophysical Research Letters*, 37, L11301, doi:10.1029/2010GL042908..

[6] Cormier, V. F. (2015), Detection of inner core solidification from observations of antipodal PKIIKP, *Geophysical Research Letters*, 42, doi:10.1002/2015GL065367.

[7] Tsuboi, S. and R. Butler, 2020. Inner core differential rotation rate inferred from antipodal seismic observations. *Physics of Earth and Planetary Interiors*, 301, April 2020, 106451, doi.org/10.1016/j.pepi.2020.106451

[8] Butler, R. and S. Tsuboi, 2020. Antipodal Observations of Global Differential Times of Diffracted *P* and *PKPAB* within the D" Layer above Earth's Core-Mantle Boundary, *Geophysical Journal International*, 220, Accepted 2020 March 27, doi.org/10.1093/gji/ggaa157

[9] Gutenberg, B., 1914. On earthquake waves, VII A. Observations on registrations of long-distance earthquakes in Göttingen and inference on the constitution of the earth (in German). Nachrichten von der Gesellschaft der Wissenschaften zu Göttingen, *Mathematisch-Physikalische Klasse* , pp. 125-176.

[10] Guttenberg, B., 1960. The shadow of the Earth's core. *Journal of Geophysical Research*, 65(3), pp.1013-1020.

[11] Brune, J.N., 1964. Travel times, body waves, and normal modes of the earth. *Bulletin of the Seismological Society of America*, 54(6A), pp.2099-2128.

[12] Brune, J.N., Nafe, J.E. & Alsop, L.E., 1961. The polar phase shift of surface waves on a sphere. Bulletin of the Seismological Society of America, 51(2), pp.247-257.

[13] Hill, D.P., 1974. Phase shift and pulse distortion in body waves due to internal caustics. *Bulletin of the Seismological Society of America*, *64*(6), pp.1733-1742.

[14] Gilbert, F., 1976. The representation of seismic displacements in terms of travelling waves. *Geophysical Journal International*, *44*(1), pp.275-280.

[15] Komatitsch, D., & Vilotte, J.P., 1998, The spectral-element method: an efficient tool to simulate the seismic response of 2D and 3D geological structures. Bulletin of the Seismological Society of America, 88, 368–392.

[16] Komatitsch, D., Ritsema, J., & Tromp, J., 2002, The spectral-element method, Beowulf computing, and global seismology. Science 298, 1737–1742 (2002).

[17] Komatitsch, D., Tsuboi, S., & Tromp, J., 2005, "The spectral-element in seismology" in Seismic Earth: Array analysis of broadband seismograms, Levander, A., G. Nolet, G., Eds. (AGU Geophysical Monograph 157, 2005), pp. 205– 227.

[18] Schimmel, M. & H. Paulssen (1997). Noise reduction and detection of weak, coherent signals through phase-weighted stacks. Geophysical Journal International, 130, 497-505.

Antipodal Observations of Global Differential Times of Diffracted *P* and PKP_{AB} within the D″ Layer above Earth's Core-Mantle Boundary

Project Representative
Seiji Tsuboi, Center for Earth Information Science and Technology, Research Institute for Value-Added-Information Generation, Japan Agency for Marine-Earth Science and Technology

Authors
Seiji Tsuboi[*1] Rhett Butler[*2]

[*1]Center for Earth Information Science and Technology, Research Institute for Value-Added-Information Generation, Japan Agency for Marine-Earth Science and Technology, [*2]University of Hawai'i

Antipodal diffracted, compressional wave (P_diff) data analyzed diametrically opposite three large earthquakes have uniformly sampled 99% of the laterally heterogeneous zone above Earth's Core–Mantle Boundary (D″ in seismic nomenclature). We use for the first time the seismic phase PKP_{AB} as a reference, which travels an identical mantle path as P_{diff}, thereby canceling common mantle heterogeneity. Essential to this research is the determination of the phase shift for P_{diff} at the antipode in order to measure differential travel times of $PKP_{AB}-P_{diff}$. Utilizing the Earth Simulator, we have independently confirmed the $\pi/4$ polar phase shift of P_{diff} at the antipode. As the 99% global P_{diff} coverage fits prior P_{diff} studies dominated by northern hemisphere paths—it implies that complementary, southern hemisphere paths must have comparable properties. Hence, the heterogeneous processes already observed in D″ may be broadly ascribed where D″ coverage has been lacking or poorly resolved.

Keywords: Numerical modelling, Wave propagation, Core–Mantle Boundary

1. Introduction

At the antipode of an earthquake, Earth acts like a nearly spherical lens focusing seismic energy through an axis-symmetric region about the diameter between the earthquake and its antipode (Figure 1). Antipodal observations [1-7] have the potential to illuminate global Earth structure not observable elsewhere complementing traditional body-wave and free-oscillation seismic methods.

PKIKP travels straight through the center of Earth, but is not the fastest path from an earthquake to the diametrically opposite anticenter or antipode. Rather, *P* waves diffracted (P_{diff}) around the Core-Mantle boundary (CMB) arrive earlier. The diffraction of *P*-waves by the core was noted by Gutenberg [9]. Years later, Gutenberg [10] hypothesized, "as an effect of the concentration of energy near the anticenter…Thus it follows that in great earthquakes the diffracted waves could well be observed as far as the anticenter."

2. Data

The first observation of antipodal P_{diff} was made by Rial [1] for an M_S=7.1 New Zealand earthquake in 1968 observed at PTO, Spain, at 179.25°Δ distance, and modeled by Rial & Cormier [2]. Butler [3] measured a *PKIKP*-P_{diff} differential travel time and polarization at PTGA antipodal (179.9°Δ) to a Mw=7.9 Minahassa Earthquake. This study extends Butler [4], incorporating two additional large earthquakes antipodal to TAM Algeria and QIZ China, and using PKP_{AB} as the P_{diff} reference phase. The combined Fresnel zone for P_{diff} from these three events covers >99% of the CMB–D" spherical shell.

3. P_{diff} and the Core–Mantle Boundary Region

The lowermost mantle, termed D″ for historical reasons borders Earth's liquid outer core. The region has been found to be significantly and laterally heterogeneous, and characterized by negative, near-zero, or positive seismic velocity gradients in different regions sampled by seismic body waves.

Prior P_{diff} research has been limited to distances short of the antipode (≤ 160 Δ°) [8-34]. Theoretical analyses of P_{diff} include [13-18, 35-38].

4. Differential travel times and phase shifts

Differential travel times have the advantage of removing common mantle heterogeneity. In this analysis PKP_{AB} is the primary reference phase, sharing the same ray surface in the mantle with P_{diff} . Where PKP_{AB} refracts into the core, P_{diff} diffracts around the core (Figure 1). Both phases join together again in transiting through the mantle from the CMB.

PKIKP is not amplified at the antipode, nor does it experience any phase shift in propagation. Both PKP_{AB} and P_{diff} are amplified (Rial & Cormier, 1980, Butler, 1986). PKP_{AB} is phase shifted $\pi/2$ radians in propagation and experiences an additional polar phase shift [39-41] of $\pi/4$ radians at 180°. The origin of the $\pi/4$ polar phase shift at the antipode is the merger of wavefields approaching (Δ<180°) the antipode (0° shifted) and the wavefields departing (Δ>180°) the

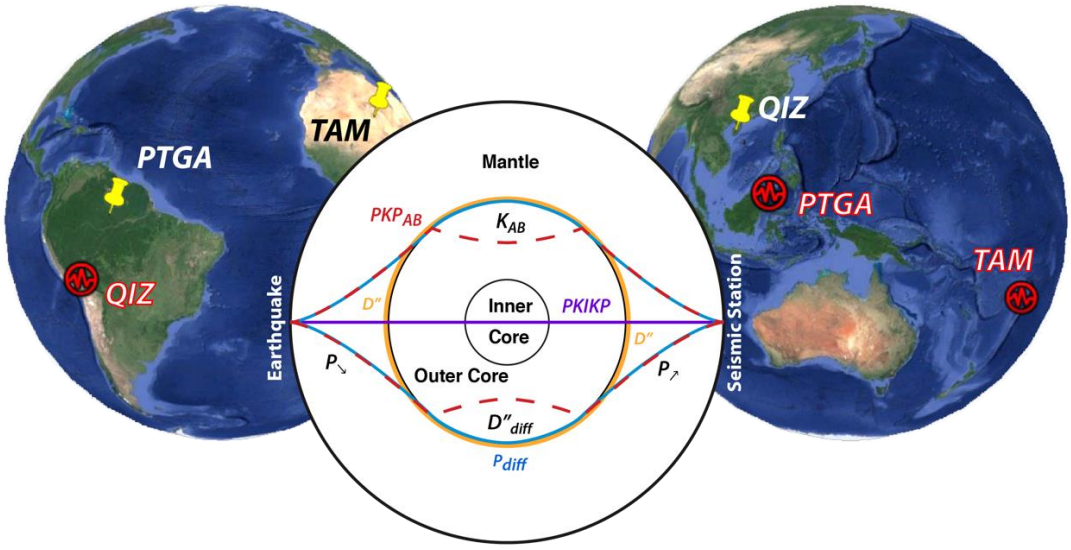

Figure 1. Maps show the locations of earthquakes (red symbols) and corresponding antipodal stations (names highlighted in red). The locations of the antipodal seismic stations are shown (yellow pins). Inset figure shows the ray paths for *PKIKP* (violet), *PKPAB* (dotted red), and P_{diff} (blue). Path segments are labeled in black. P_{diff} and *PKPAB* share the same *P*-wave ray parameter and path in the mantle, indicated by down-going $P_{\searrow}$ and up-going $P_{\nearrow}$. The outer core segment of *PKPAB* is labeled K_{AB}. The D″ region at the base of the mantle is shown (orange), where D''_{diff} is the CMB diffracted segment of P_{diff}. Although ray paths are shown in this cross-section, the antipodal energy arrives from all azimuths as a ray surface.

antipode (90° shifted), combining at the antipode (Δ=180°) to a net $\pi/4$ or 45° phase shift.

The determination of differential seismic travel times requires consistency in the phase of the compared arrivals. To compare waveforms, the phases must be adjusted to a common basis. Therefore, a key question is whether or not P_{diff} experiences the same $\pi/4$ radians, polar phase shift as PKP_{AB}.

5. P_{diff} polar phase shift computation

Brune [39] & Gilbert [42] both discussed the applicability of the polar phase shift for normal modes. In principle, since P_{diff} may be considered as a sum of normal modes, the polar phase shift follows naturally. Hill [41] viewed the polar phase shift (axial caustic) as a ray-theoretical, high-frequency phenomenon.

Since the polar phase shift of P_{diff} has not been confirmed theoretically—bridging from high-frequency optics to long-period surface-waves & normal modes—we approached the problem synthetically using the Spectra Element Method (SEM) [5, 43-45]. By directly comparing P_{diff} and PKP_{AB} computed for a true, 3D spherical PREM model at exactly 180°Δ diametrally opposite an isotropic explosion source, we include any asymptotic, frequency-dependent phase implicitly.

In modeling the P_{diff} phase, we use a mesh with a total of 13.5 billion global integration grid points, which corresponds to an approximate grid spacing of 2.0 km along the Earth's surface and provides for synthetics seismograms accurate up to 3.5 seconds.

6. P_{diff} polar phase shift measurement

The results of this synthesis are shown in Figure 2 for two alternatives: P_{diff} either is polar phase shifted $\pi/4$ (45°) or not (0°). Firstly, $[PKP_{AB}]\_(-\pi/2)$ is phase shifted by $-\pi/2$ radians (to account for the PKP_{AB} propagation caustic) and compared directly with P_{diff}. No correction is made for a polar phase shift. Since $[PKP_{AB}]\_(-\pi/2)$ implicitly contains the $\pi/4$ polar phase shift, the concomitant fit to P_{diff} stipulates that P_{diff} implicitly contains the same polar phase shift. Alternatively, $[PKP_{AB}]\_(-3\pi/4)$ is phase shifted $-3\pi/4$ radians correcting for both the polar phase shift and propagation caustic. Since $[PKP_{AB}]\_(-3\pi/4)$ explicitly reversed the PKP_{AB} $(\pi/4)$ polar phase shift, a close fit between P_{diff} and $[PKP_{AB}]\_(-3\pi/4)$ implies that P_{diff}

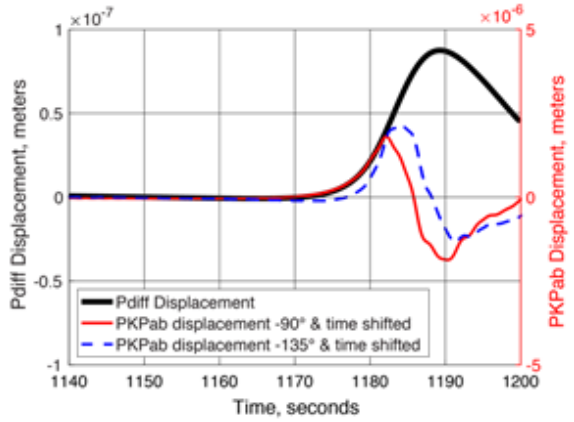

Figure 2(a) Synthetic displacement waveform comparisons are computed for a spherical PREM Earth model by the Spectral Element Method (SEM) in order to resolve a potential polar phase shift in P_{diff} at the antipode, Δ=180°. Qualitatively, [PKP$_{AB}$]_$(-\pi/2)$ initially overlays P_{diff}, whereas [PKP$_{AB}$]_$(-3\pi/4)$ fits poorly. The close waveform correspondence of P_{diff} and $[PKP_{AB}]\_(-\pi/2)$ breaks down ~15 seconds later upon arrival of shorter-period components of PKP_{AB} likely originating in D″.

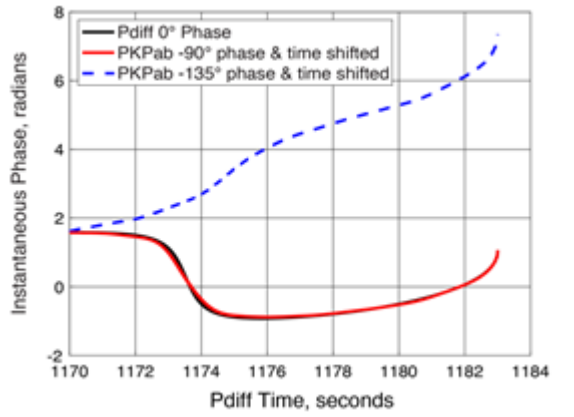

Figure 2(b) The instantaneous phase is shown, derived from the displacement components. P_{diff} (black) and $[PKP_{AB}]\_(-\pi/2)$ (red) overlay one another. However, P_{diff} and $[PKP_{AB}]\_(-3\pi/4)$ (blue dotted) compare poorly. Therefore, P_{diff} and $[PKP_{AB}]\_(-\pi/2)$ possess the nearly the same instantaneous phase at the beginning of the P_{diff}window, corroborating a P_{diff} polar phase shift of $(\pi/4)$ at the antipode.

lacks the polar phase shift. However, since the fit is poor the inference is that P_{diff} does have a polar phase shift.

Instantaneous phase [46] is plotted in Figure 2b. Similar to the comparison in Figure 2a, [PKP$_{AB}$]_$(-\pi/2)$ overlays P_{diff}, sharing the same phase relation. Furthermore, [PKP$_{AB}$]_$(-3\pi/4)$ fits poorly. Therefore, the instantaneous phases indicate that [PKP$_{AB}$]_$(-\pi/2)$ overlays P_{diff} and both share the same polar phase shift. That this polar phase shift is $\frac{\pi}{4}$ is seen in comparison between antipodal observations of PKIKP and PKP$_{AB}$ in Figure 3 row 3. Since PKIKP experiences no polar nor propagation phase shift, yet matches PKP$_{AB}$ phase shifted by $(-\pi/2-\pi/4)=-3\pi/4$ radians, confirms the antipodal polar phase shift of $\pi/4$ for PKP$_{AB}$, and hence an antipodal polar phase shift of $\pi/4$ for P_{diff}.

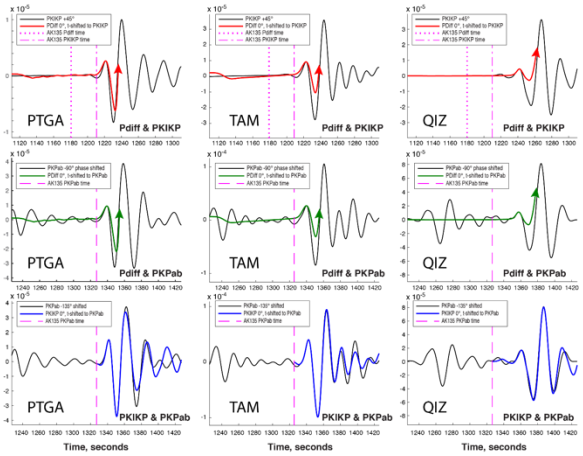

Figure 3. Three velocity waveform comparisons (noted in lower right of inset) are shown for PTGA (left column), TAM (center column), and QIZ (right column). The rows show the waveform fits—correlated by their initial peaks—among the P_{diff}, *PKIKP*, and PKP_{AB} arrivals: (top) P_{diff} & *PKIKP*; (middle) P_{diff} & PKP_{AB}; and (bottom) *PKIKP* & PKP_{AB}. Within each inset legend, the phase shift corrections applied to *PKIKP* or PKP_{AB} are indicated. The energetic arrival of *PKIKP* following P_{diff} is indicated by the arrow upwards. The close overlay of *PKIKP* with PKP_{AB} in the bottom row shows that the modeled $(-\pi/2-\pi/4)$ PKP_{AB} phase shift is consistent with a $(\pi/4)$ polar phase shift at 180°Δ.

7. P_{diff} or PKP$_{AB}$ heterogeneity

The $PKP_{AB}-P_{diff}$ time (Figure 1) is the difference between the time along the outer core path (K_{AB}) and

path of diffracted *P* in D″ near the CMB (termed D_{diff} for convenience). The mantle paths *(P)*, which are nearly identical, are thereby subtracted. This gross earth datum is independent of an Earth model. To separate the contributions of D_{diff} from K_{AB}, we must resort to an Earth model. This is reasonable since the outer core is considered to be laterally homogeneous and well mixed [47].

Since travel times are most sensitive to the ray parameter at its turning point, allocating part of the differential time to K_{AB}, which bottoms in the middle of the Outer Core, implies that the Core velocity is modified. The middle of the Outer Core is far from the possible heterogeneity at the CMB and IOCB. Multiple seismic phases have the same ray parameter and bottom at the same depth as PKP_{AB}—including $PKKS_{AB}$ and $SKKP_{AB}$ (142°), SKP_{AB} and PKS_{AB} (140°), SKS_{AC} (105°)and $PKKP_{AB}$ (107°), $SKKS_{AC}$ (175°)—and thereby constrain the PKP_{AB} (180°) velocity at its turning point. Nonetheless, there is no significant evidence for heterogeneity within the middle of the Outer Core [48-50].

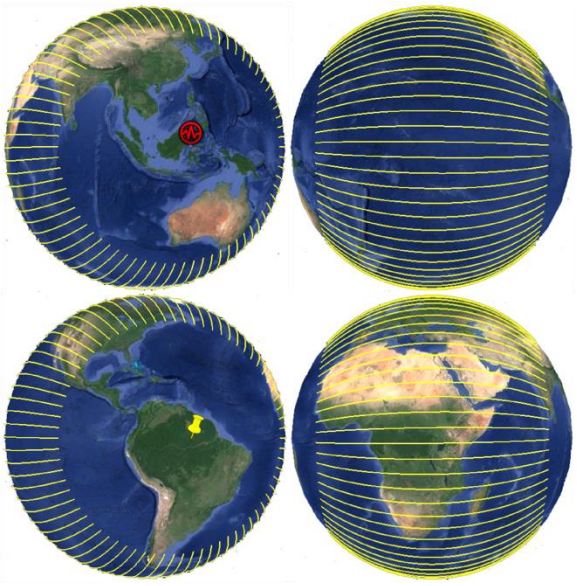

Figure 4. The P_{diff} Fresnel zone is projected as a striped surface for the 1996 antipodal pair: PTGA, yellow pin; Minahassa earthquake, red wavelet. The yellow minor arcs mark the propagation path of the P_{diff} ray sheet in D″, highlighted at 5° intervals. The left figures are rotated slightly to enhance the curvature.

8. Fresnel zone of P_{diff}

The breadth of the Fresnel zone of P_{diff} has been considered in several studies [4, 23, 28, 32-34]. At the antipode, the Fresnel zone at the CMB encompasses an annular zone between the small circles which define the entry and exit of PKP_{AB} at the CMB. For PTGA the Fresnel zone is shown in Figure 4 reflects the substantial coverage of the CMB at the antipode. However, the near-source and near-receiver "caps" of the zone are not sampled.

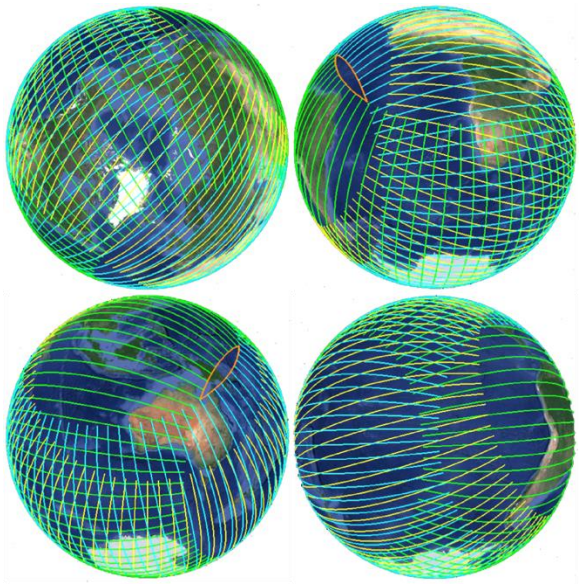

Figure 5. Tetrahedral views of P_{diff} coverage of the CMB plot the overlapping Fresnel zones for the three diametral axes. Center of projections clockwise from top left: (90° 0°), (-30° 0°), (-30°, 120°), and (-30° -120°). Individual ray sheets are plotted with 5° ray spacing, where yellow corresponds with PTGA–Brazil, green is for TAM–Tonga, and cyan is for QIZ–North Chile. Note the slivers without coverage outlined in orange east of South America (top right) and northeast of Australia (lower left). The combined P_{diff} coverage by PTGA, TAM, and QIZ encompasses 99.5% of the CMB and D″.

The two additional antipodal pairs, TAM–Tonga and QIZ–Chile, provide independent corroboration of the insights gained from PTGA, and more importantly, coverage of the CMB missed by PTGA P_{diff}. The combined coverage of PTGA, TAM, and QIZ envelopes is >99% of D″ and the CMB (Figure 5).

Although we cannot illuminate CMB D″ fine structure with P_{diff}, the antipodal view afforded by P_{diff} and PKP_{AB} provides for a strong constraint on its global, mean velocity characteristics. It follows that the heterogeneities characteristic of CMB D″ observed where good seismological coverage is available may also be ascribed where coverage has been lacking.

9. Conclusion

The Earth Simulator has been utilized for determining important, subtle phase shifts in seismic waves diffracting in the base of the mantle around Earth's outer core—essential for measuring the global mean velocity at the core-mantle boundary. This global measure samples 99% of this strongly heterogeneous region. This is the first constraint of diffraction at the antipode, linking theoretical asymptotic, frequency dependence. The next phase of analysis will incorporate 3D structure within the Inner Core to extend the methodology to five antipodal diameters measuring propagation within and diffraction around the Inner Core.

Acknowledgement

We used seismic data provided by Geoscope and the Global Seismographic Network. Computations were conducted on the Earth Simulator at the Japan Agency for Marine-Earth Science and Technology.

References

[1] Rial, J. A., 1979. Seismic waves at the epicenter's antipode, Doctoral Dissertation Caltech, Pasadena.

[2] Rial, J. A., and V. F. Cormier, 1980. Seismic waves at the epicenter's antipode, *J. Geophys. Res.*, *85*, 2661–2668.

[3] Butler, R., 1986. Amplitudes at the antipode, *Bulletin of the Seismological Society of America*, *76*, 1355–1365.

[4] Butler, R., 1998. Antipodal observations of the inner-outer core boundary and diffracted P, *EOS Trans. AGU suppl*., 79.

[5] Butler, R., and S. Tsuboi, 2010. Antipodal seismic observations of temporal and global variation at Earth's inner-outer core boundary, *Geophysical Research Letters*, 37, L11301, doi:10.1029/2010GL042908..

[6] Cormier, V. F. (2015), Detection of inner core solidification from observations of antipodal PKIIKP, *Geophysical Research Letters*, 42, doi:10.1002/2015GL065367.

[7] Tsuboi, S. and R. Butler, 2020. Inner core differential rotation rate inferred from antipodal seismic observations. *Physics of Earth and Planetary Interiors*, 301, April 2020, 106451, doi.org/10.1016/j.pepi.2020.106451

[8] Butler, R. and S. Tsuboi, 2020. Antipodal Observations of Global Differential Times of Diffracted *P* and *PKPAB* within the D" Layer above Earth's Core-Mantle Boundary, *Geophysical Journal International*, 220, Accepted 2020 March 27, doi.org/10.1093/gji/ggaa157

[9] Gutenberg, B., 1914. On earthquake waves, VII A. Observations on registrations of long-distance earthquakes in Göttingen and inference on the constitution of the earth (in German). Nachrichten von der Gesellschaft der Wissenschaften zu Göttingen, *Mathematisch-Physikalische Klasse* , pp. 125-176.

[10] Guttenberg, B., 1960. The shadow of the Earth's core. *Journal of Geophysical Research*, 65(3), pp.1013-1020.

[11] Sacks, S., 1967. Diffracted P-wave studies of the Earth's core: 2. Lower mantle velocity, core size, lower mantle structure. *Journal of Geophysical Research*, 72(10), pp.2589-2594.

[12] Sacks, S., 1966. Diffracted wave studies of the Earth's core: 1. Amplitudes, core size, and rigidity. *Journal of Geophysical Research*, 71(4), pp.1173-1181.

[13] Phinney, R.A. & Alexander, S.S., 1966. P wave diffraction theory and the structure of the core-mantle boundary. *Journal of Geophysical Research*, 71(24), pp.5959-5975.

[14] Phinney, R.A. & Alexander, S.S., 1969. The effect of a velocity gradient at the base of the mantle on diffracted P waves in the shadow. *Journal of Geophysical Research*, 74(20), pp.4967-4971.

[15] Alexander, S.S. & Phinney, R.A., 1966. A study of the core-mantle boundary using P waves diffracted by the Earth's core. *Journal of Geophysical Research*, 71(24), pp.5943-5958.

[16] Phinney, R.A. & Cathles, L.M., 1969. Diffraction of P by the core: A study of long-period amplitudes near the edge of the shadow. *Journal of Geophysical Research*, 74(6), pp.1556-1574.

[17] Doornbos, D.J. & Mondt, J.C., 1979a. Attenuation of P and S waves diffracted around the core. *Geophysical Journal International*, 57(2), pp.353-379.

[18] Doornbos, D.J. & Mondt, J.C., 1979b. P and S waves diffracted around the core and the velocity structure at the base of the mantle. *Geophysical Journal of the Royal Astronomical Society*, 57(2), pp.381-395.

[19] Mula, A.H.G., 1981. Amplitudes of diffracted long-period P and S waves and the velocities and Q structure at the base of the mantle. *Journal of Geophysical Research: Solid Earth*, 86(B6), pp.4999-5011.

[20] Ruff, L.J. & Helmberger, D.V., 1982. The structure of the lowermost mantle determined by short-period P-wave amplitudes. *Geophysical Journal International*, 68(1), pp.95-119.

[21] Wysession, M.E. & Okal, E.A., 1989. Regional analysis of D ″velocities from the ray parameters of diffracted P profiles. *Geophysical Research Letters*, 16(12), pp.1417-1420.

[22] Wysession, M.E., Okal, E.A. & Bina, C.R., 1992. The structure of the core-mantle boundary from diffracted waves. *Journal of Geophysical Research: Solid Earth*, 97(B6), pp.8749-8764.

[23] Wysession, M.E., 1996. Large-scale structure at the core-mantle boundary from diffracted waves. *Nature*, 382(6588), pp.244-248.

[24] Wysession, M.E., Langenhorst, A., Fouch, M.J., Fischer, K.M., Al-Eqabi, G.I., Shore, P.J. & Clarke, T.J., 1999. Lateral variations in compressional/shear velocities at the base of the mantle. *Science*, 284(5411), pp.120-125.

[25] Souriau, A. & Poupinet, G., 1994. Lateral variations in P velocity and attenuation in the D″ layer, from diffracted P waves. *Physics of the Earth and Planetary Interiors*, 84(1-4), pp.227-234.

[26] Bataille, K. & Lund, F., 1996. Strong scattering of short-period seismic waves by the core-mantle boundary and the P-diffracted wave. *Geophysical Research Letters*, 23(18), pp.2413-2416.

[27] Hock, S., Roth, M. & Müller, G., 1997. Long-period ray parameters of the core diffraction P diff and mantle heterogeneity. *Journal of Geophysical Research: Solid Earth*, 102(B8), pp.17843-17856.

[28] Sylvander, M., Ponce, B. & Souriau, A., 1997. Seismic velocities at the core-mantle boundary inferred from P waves diffracted around the core. *Physics of the Earth and Planetary Interiors*, 101(3-4), pp.189-202.

[29] Kárason, H. & van der Hilst, R.D., 2001. Tomographic imaging of the lowermost mantle with differential times of refracted and diffracted core phases (PKP, P_{diff}). *Journal of Geophysical Research: Solid Earth*, 106(B4), pp.6569-6587.

[30] Ritsema, J. & van Heijst, H.J., 2002. Constraints on the correlation of P-and S-wave velocity heterogeneity in the mantle from P, PP, PPP and PKP ab travel times. *Geophysical Journal International*, 149(2), pp.482-489.

[31] Koelemeijer, P., Deuss, A. & Ritsema, J., 2013. Observations of core-mantle boundary Stoneley modes. *Geophysical Research Letters*, 40(11), pp.2557-2561.

[32] Hosseini, K. & Sigloch, K., 2015. Multifrequency measurements of core-diffracted P waves (P_{diff}) for global waveform tomography. *Geophysical Journal International*, 203(1), pp.506-521.

[33] Euler, G.G. & Wysession, M.E., 2017. Geographic variations in lowermost mantle structure from the ray parameters and decay constants of core-diffracted waves. *Journal of Geophysical Research: Solid Earth*, 122(7), pp.5369-5394.

[34] Hosseini, K., Sigloch, K., Tsekhmistrenko, M., Zaheri, A., Nissen-Meyer, T. & Igel, H., 2019. Global mantle structure from multifrequency tomography using P, PP and P-diffracted waves. *Geophysical Journal International*, *220*(1), pp.96-141.

[35] Scholte, J. G. J., 1956. *On seismic waves in a spherical Earth*, Royal Nederlandsche Meteorological Institute, Publication 65:1-55.

[36] Knopoff, L. & Gilbert, F., 1961. Diffraction of elastic waves by the core of the earth. *Bulletin of the Seismological Society of America*, 51(1), pp.35-49.

[37] Mula, A.H. & Müller, G., 1980. Ray parameters of diffracted long period P and S waves and the velocities at the base of the mantle. *Pure and Applied Geophysics*, 118(2), pp.1272-1292.

[38] Aki, K. & Richards, P G., 1980. *Quantitative seismology Theory and methods*. Vol. 1, WH Freeman, San Francisco. 557 pp.

[39] Brune, J.N., 1964. Travel times, body waves, and normal modes of the earth. *Bulletin of the Seismological Society of America*, 54(6A), pp.2099-2128.

[40] Brune, J.N., Nafe, J.E. & Alsop, L.E., 1961. The polar phase shift of surface waves on a sphere. *Bulletin of the Seismological Society of America*, 51(2), pp.247-257.

[41] Hill, D.P., 1974. Phase shift and pulse distortion in body waves due to internal caustics. *Bulletin of the Seismological Society of America*, *64*(6), pp.1733-1742.

[42] Gilbert, F., 1976. The representation of seismic displacements in terms of travelling waves. *Geophysical Journal International*, *44*(1), pp.275-280.

[43] Komatitsch, D., & Vilotte, J.P., 1998, The spectral-element method: an efficient tool to simulate the seismic response of 2D and 3D geological structures. *Bulletin of the Seismological Society of America*, 88, 368–392.

[44] Komatitsch, D., Ritsema, J., & Tromp, J., 2002, The spectral-element method, Beowulf computing, and global seismology. *Science* 298, 1737–1742 (2002).

[45] Komatitsch, D., Tsuboi, S., & Tromp, J., 2005, "The spectral-element in seismology" in *Seismic Earth: Array analysis of broadband seismograms*, Levander, A., G. Nolet, G., Eds. (*AGU Geophysical Monograph* 157, 2005), pp. 205– 227.

[46] Schimmel, M. & H. Paulssen (1997). Noise reduction and detection of weak, coherent signals through phase-weighted stacks. *Geophysical Journal International*, 130, 497-505.

[47] Stevenson, D.J., 1987. Limits on lateral density and velocity variations in the Earth's outer core. *Geophysical Journal International*, 88(1), pp.311-319.

[48] Morelli, A. and Dziewonski, A.M., 1987. Topography of the core–mantle boundary and lateral homogeneity of the liquid core. *Nature*, *325*(6106), pp.678-683.

[49] Souriau, A., Teste, A. and Chevrot, S., 2003. Is there any structure inside the liquid outer core?. *Geophysical research letters*, *30*(11).

[50] Dai, W. and Song, X., 2008. Detection of motion and heterogeneity in Earth's liquid outer core. *Geophysical research letters*, *35*(16).